

# Performance Evaluation of Gun Damping Systems with Variable Recoil Length and Spring-Loaded Valves

Mohamed Abdullah, Wael Elsaady\*, Ahmed Ibrahim and Ibrahim Elsherif

*Mechanical Engineering Branch, Military Technical College, Cairo, 11766, Egypt*

*\*E-mail: wael.elsaady@mtc.edu.eg*

## ABSTRACT

This paper presents modelling analysis and experimental testing of the performance of gun recoil system provided with variable recoil length and braked recuperator. The gun recoil cycle is studied considering the effect of presence of spring-loaded valve (SLV) in recoil system. A mathematical model has been developed using MATLAB/Simulink for the 130 mm M-46 Field Gun (FG). The model is validated by comparing theoretical recoil parameters with experimental data measured due to real firing tests. The firing tests were implemented for a new self-propelled system of the 130 mm FG that was designed and manufactured by the Egyptian Armed Forces. The results indicate that the recoil parameters are highly affected by the presence of the SLV. It has been found that the measured Counter-Recoil (CR) velocity is about 11 % less than its counterpart predicted by the mathematical model without considering the effect of SLV. In addition, the driving force during CR is predicted to be 33 % less compared to that without considering the effect of SLV. This causes the duration of CR time period to be 10 % longer and the resistance against CR to be about 20 % less compared to these values without considering the effect of SLV.

**Keywords:** Braked recuperator; Variable recoil; Shock absorber; Spring-loaded valve; Control recoil mechanism

## NOMENCLATURE

$A_{2T}$	: Cross-section area of CRM cylinder
$L_V$	: Length of valve hole
$A_{IP}$	: Working area of CRM piston
$m_R$	: Mass of gun recoiling parts
$A_{PB}$	: Working area of RM pistons
$n$	: Polytropic exponent
$A_{PR}$	: Recuperator working area
$n_h$	: Number of holes in recuperator valve
$A_x$	: Throttling area during recoil
$P_{air}$	: Air pressure force
$A_{xc}$	: Throttling area during CR
$P_B$	: Force of powder gases
$C_2$ & $C_3$	: Recoil constants
$P_R$	: Recuperator force
$c_s$	: Damping coefficient of cradle seat
$P_{Ro}$	: Initial recuperator force
$d_{v_h}$	: Diameter of recuperator valve hole
$p_1, p_2, p_3$	: Liquid pressures in Zones 1, 2 & 3 of recoil brake
$F_{lossesCR}$	: Recuperator losses during CR
$R_f$	: Total friction resistances
$F_{lossesR}$	: Recuperator losses during recoil
$V$	: Recoil velocity
$F_{rec}$	: Recuperator force
$V_{Ro}$	: Initial air volume
$F_{seat}$	: Cradle seat reaction

$v_F$	: Velocity of flow in recoil brake
$f$	: Coefficient of friction of flow in recuperator valve
$X$	: Recoil distance
$K$	: Total hydraulic resistance during recoil.
$\xi_1$	: Coefficient of losses in recuperator SLV
$K_C$	: Total hydraulic resistance during CR.
$\rho_L$	: Liquid density
$k_s$	: Stiffness of cradle seat
$\varphi$	: Elevation angle
$k_{valve}$	: Stiffness of valve spring
$\Omega_{min}$	: Minimum area for liquid flow from Zone 1 to 3

## 1. INTRODUCTION

Gun recoil cycle is characterised by the backward and forward motion of gun recoiling parts due to firing. Comparing with non-recoiling weapon systems, gun recoil reduces total force imparted to gun carriage<sup>1-3</sup>. Typically, a gun recoil system consists of three main mechanisms, namely: Recoil Mechanism (RM) that dissipates the major part of recoil energy, recuperator that accumulates part of this energy to be used for Counter-Recoil (CR), and Control Recoil Mechanism (CRM) that brakes gun recoiling parts during CR. There are some constructions of recuperators that may be also functioned to dissipate some of CR energy. These recuperators can be termed as “braked” recuperators, whose study is the main subject of this paper.

Zhang<sup>4</sup>, *et al.* constructed an analytical method to identify the error between theoretical and experimental gun

recoil displacements. Elsaady<sup>5</sup>, *et al.* studied the dynamic characteristics of the recoil system of the 120-mm M256 tank gun using MATLAB/Simulink. Balla<sup>6</sup>, *et al.* studied the recoil system located in the 125 mm tank gun. In both studies, the recoil parameters were determined using analytical dynamic models, and the models were validated by experimental measurements. Miao<sup>7</sup>, *et al.* studied the recoil parameters of the RM of the 155 mm howitzer.

In contrast to the analytical models discussed above, numerical models allow the study of the flow of liquid due to gun recoil as multi-dimensional, turbulent, compressible, and unsteady flow problems<sup>8-12</sup>. Therefore, more characteristics can be accounted for in these models. Huan<sup>12</sup>, *et al.* studied the flow characteristics of highly nonlinear elastic colloid gel in gun recoil systems using ANSYS/Fluent software. It should be noted that other types of gun recoil systems can be termed “smart recoil systems”, in which implementation of numerical approaches is reported to be better. The smartness of these recoil systems is manifested by their ability to considerably control the recoil parameters and minimise the recoil impulse. Examples of these types are soft recoil systems<sup>1,8,13</sup> and Magneto-Rheological (MR) gun recoil systems<sup>9-11</sup>.

It can be analysed from the available literature that the damping resistances of the recuperator and RM are either modelled by the determination of the equivalent damping coefficient of the recoil system, or by the analysis of flow and energy equations in recuperator and RM. However, simulation of gun recoil cycle considering the effects of presence of braked recuperators are, to the best of the author’s knowledge, not discussed in the literature. Moreover, modelling of the performance of recoil systems with variable recoil length is not frequently discussed. Therefore, this paper aims to study these effects utilising the 130 mm M-46 FG provided with braked recuperator and recoil system of variable recoil length.

**2. CONSTRUCTION OF RECOIL SYSTEM**

**2.1 Recuperator**

The recuperator of 130 mm FG can be classified as a hydro-pneumatic braked recuperator whose piston is fixed to the cradle and the cylinder recoil with the barrel assembly. The working cylinder is located eccentrically inside the air

cylinder, as shown in Figure 1. The working cylinder is full of liquid, whereas the air cylinder is partially filled with liquid whose level initially locates at the axis of the working cylinder. The air cylinder traps compressed air/nitrogen that provides necessary energy for fixing gun recoiling parts at their most forward position. An intermediate cylinder is located between the working and air cylinders to prevent escaping of air from outer cylinder into the working cylinder at high elevation angles.

The braking function of recuperator during recoil cycle is shown schematically by the positions of the Spring-Loaded Valve (SLV) seen in Fig. 1. The SLV is a one-way valve that opens during recoil causing the liquid to flow around the valve (Flow A) to compress the air located in the air cylinder. During CR, the valve closes causing the liquid to flow from the small openings located in the valve (Flow B) under the effect of compressed air.

**2.2 Recoil Mechanism**

Figure 2 shows the RM of the 130 mm FG. Part (a) of this figure shows a 2D schematic drawing of the RM, whereas Part (b) and (c) show the flow paths of liquid during recoil cycle in the locations of RM piston and CRM valve, respectively. The RM is mainly composed of a piston-cylinder system; the piston rod is hollow and it works as a working cylinder for the CRM. The piston rod is fixed to the gun recoiling parts, and the cylinder is fixed to the cradle.

In order to illustrate the function of RM during the recoil cycle, the following zones, seen in Fig. 2, are denoted: (i) Zone 1: represents the fluid volume in RM cylinder behind the piston, (ii) Zone 2: represents the fluid volume in RM cylinder in front of the piston, and (iii) Zone 3: represents the fluid volume in the piston cavity. In addition, there are five flow paths of the liquid shown on the figure, termed as: Flow A to E. The throttling areas that compose these flow paths are described as follows: (i) the short recoil grooves (paths of Flow A) are six longitudinal grooves in RM cylinder of 30 mm constant width and variable depth ranging from 1.5 to 3 mm, (ii) the long recoil grooves (paths of Flow B) are four longitudinal grooves milled on the external surface of the throttling rod. The width

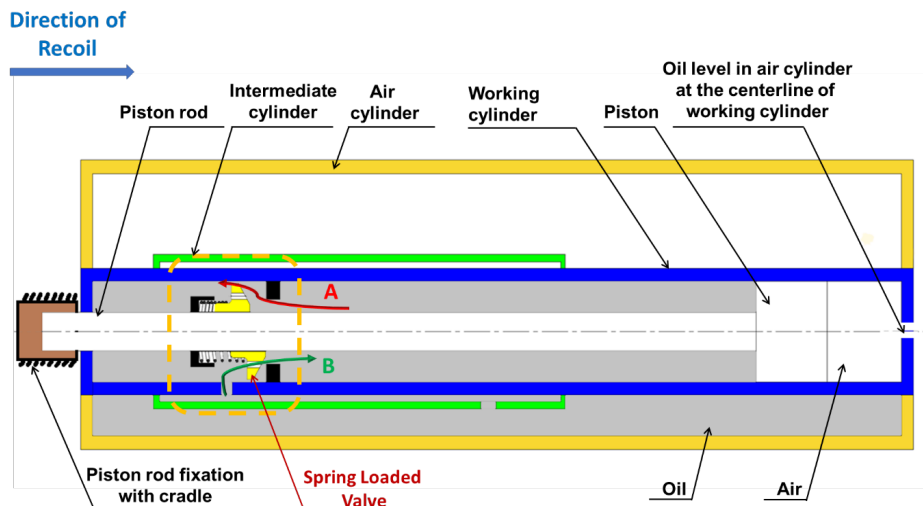


Figure 1. Hydro-pneumatic braked recuperator.

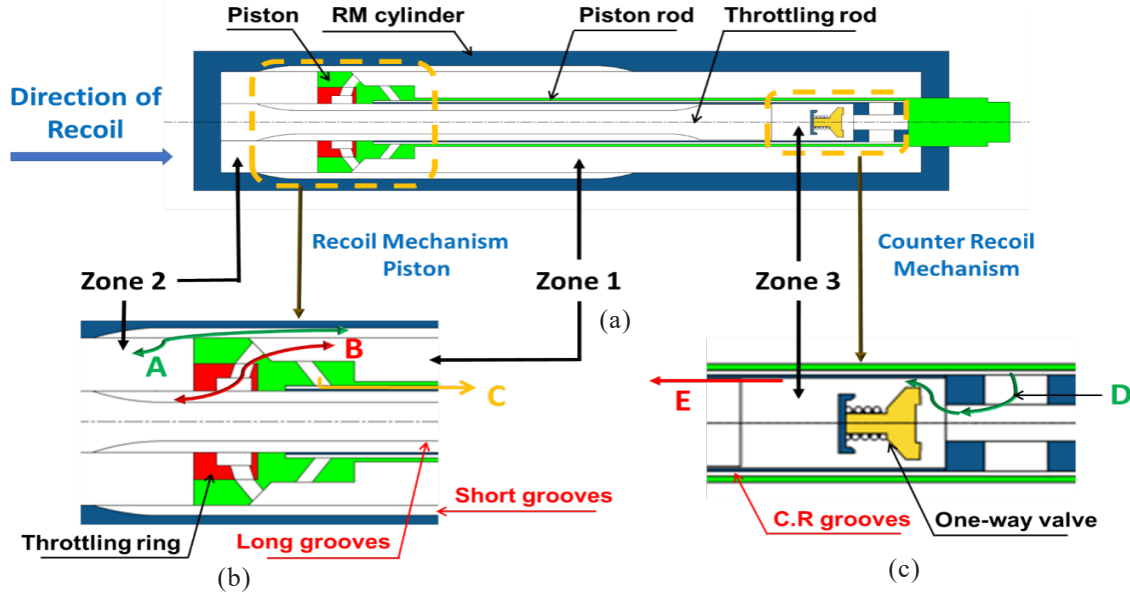


Figure 2. Recoil mechanism with variable recoil length of the 130 mm FG: (a) 2D view of RM in which the fluid occupies three main zones, (b) and (c) detailed views of the RM piston and the CRM valve, respectively.

Table 1. Data of variable recoil lengths in correspondence to elevation angles, active throttling areas and flow paths.

	Long recoil	Intermediate recoil	Short recoil
Recoil length	$\Lambda_L=1250$ mm	$\Lambda=780:1250$ mm	$\Lambda_S=780$ mm
Operating angles	$(0 \leq \varphi \leq 20^\circ)$	$(20^\circ \leq \varphi \leq 34^\circ)$	$(34^\circ \leq \varphi \leq 45^\circ)$
Active flow paths during recoil	A, B, C, D	A, B, C, D	A, C, D
Active flow paths during CR	A, B, E	A, B, E	A, E
Throttling area ( $A_x$ )	$A_{XL}+A_{Xsh}$	$\left(\frac{(34-\varphi)}{14}A_{XL}+A_{Xsh}\right)$	$A_{Xsh}$

of the grooves is 20 mm, whereas their depth is 9 mm, and (iii) the CR grooves (paths of Flow E) are two longitudinal grooves of 20 mm width and 0.4 mm depth. Flow C describes the flow in the piston cavity around the CRM, and it extends as Flow D around the one-way valve of CRM.

During recoil, the pressure in Zone 1 builds up, and the liquid is forced to flow from Zone 1 to Zone 2 from two paths, namely: (i) Flow A from the short recoil grooves, and (ii) Flow B through the inclined holes in the piston head, the openings in the intermediate throttling ring, and through the long grooves. In addition, the liquid flows from Zone 1 to Zone 3 (Flow C and D). The resistances due to Flow A and B produce the main part of recoil resistance.

During CR, the liquid flows back from Zones 2 and 3 to Zone 1. Flow A and B are reversed to manifest the flow between Zone 2 to 1. However, the liquid flows between Zone 3 to 1 through the CR grooves, Flow E, as the reversed Flow D is blocked by the one-way valve in CRM. The resistances to Flow A, B, and E produce the hydraulic resistance during CR.

The availability of variable recoil length is achieved by controlling the throttling area from which the liquid flows. The throttling area is controlled by a mechanism that leads the throttling rod to rotate around its axis at high elevation angles. This rotation leads to gradual blocking of the path of Flow B between the throttling ring and the throttling rod. In terms of gun specifications listed in the gun service manual, the data

of the 130 mm FG at different recoil lengths corresponding to elevation angles and active throttling areas are listed in Table 1.

### 3. MATHEMATICAL MODEL

The recoil parameters during the recoil cycle are determined by solving the equation of motion of recoiling parts during recoil cycle, written as follows<sup>5</sup>:

$$m_R \frac{d^2 X}{dt^2} = m_R \frac{dV}{dt} = P_B - K - P_R - R_f - F_{seat} + m_R g \sin \varphi \quad (1)$$

where,  $m_R$  is the mass of recoiling parts,  $X$  is the recoil displacement,  $V$  is the recoil velocity,  $t$  is time,  $\varphi$  is the elevating angle,  $P_B$  is the force of powder gases,  $K$  is the hydraulic resistance of RM,  $P_R$  is the recuperator force,  $R_f$  is the total friction resistance.  $R_f$  is assumed to be constant, as it is reported to have a very limited contribution to the total recoil resistance<sup>5-6</sup>.  $F_{seat}$  is the reaction that affects the recoiling parts due to their bearing on cradle seat. This reaction evolves only at  $X=0$  (before and at the end of recoil), and it is represented in the mathematical model by Eqn (2)<sup>5</sup>:

$$F_{seat} = \begin{cases} 0 & X \leq 0 \\ -k_s X - c_s V, & X > 0 \end{cases} \quad (2)$$

where,  $k_s=100$  N/m is the stiffness and  $c_s=9.0 (10^7)$  N.s/m is the damping coefficient. The values are assumed to represent the

seat as a spring-dashpot system with a very low stiffness and a very high damping coefficient. The non-inclusion of  $F_{seat}$  in the equation of motion results in the presence of illogical harmonic damped oscillations of the time history of recoil velocity.

The mathematical model has been established using MATLAB/Simulink, as shown in Fig. 3. The summation of the forces and resistances affecting the recoil cycle is divided by the recoiling mass in order to determine recoil acceleration, which is integrated with respect to time to determine the recoil velocity,  $V$ . Then, the recoil velocity,  $V$ , is integrated to determine the recoil displacement,  $X$ . In addition, since the recoil system of the 130 mm FG adopts variable recoil length, the structure of the MATLAB/Simulink model augments also the effect of change of elevation angle.

The force of powder gases is determined from the internal ballistics solution according to the data of full-charge ammunition using the ‘‘Charbonnier-Sugot’’ method<sup>14</sup>. The impulse due to discharge of powder gases after the projectile leaves the barrel is calculated using Bravin’s equation<sup>5</sup>, shown by Eqn. (3). Hence, the total force of powder gases can be determined.

$$P_B = \chi P_M e^{-\frac{t'}{b}} \tag{3}$$

where,  $\chi = \frac{I_{AA(MB)}}{I_{AA}}$  is the ratio between impulse of powder gases during period of discharge of gases with and without effect of muzzle brake,  $P_M$  is the force of powder gases at muzzle,  $b$  is Bravin’s exponent, and  $t'$  is the time of gas discharge measured from the muzzle moment. The muzzle brake parameters were calculated using the same model<sup>15</sup>,

and the values were found to be as follows:  $\chi=0.07$ ,  $P_M=104$  (MPa),  $b=0.007$ , and  $t_{EA}=0.07$  (sec), where,  $t_{EA}$  is the duration of AAPG.

The effect of the muzzle brake is determined by studying the flow of gases from the muzzle brake, following the same procedure<sup>15</sup>. In that paper, the geometrical parameters of a muzzle brake used for a sniper rifle are studied. The same system of equations discussed in Ref. 15 is adopted in this study for the geometrical parameters of the muzzle brake of the 130 mm FG.

Figure 4 shows the time history of the force of powder gases with and without considering the effect of the muzzle brake. The effect of the muzzle brake is represented by the negative impulse seen in Fig. 4. The superposition of values of the two curves represents the net impulse imparted to the gun recoiling parts. It can be analysed that the muzzle brake considerably decreases the total impulse of powder gases, as it nearly eliminates the impulse of powder gases after the projectile leaves the barrel.

### 3.1 Recuperator Force

Recuperator force,  $F_{rec}$ , depends on the instantaneous gas/air pressure force inside the recuperator,  $P_{air}$ . This pressure force can be determined as a function of recoil distance,  $X$ , as follows<sup>16</sup>:

$$P_{air} = P_{Ro} \cdot \left( \frac{V_{Ro}}{V_{Ro} - A_{PR} \cdot X} \right)^n \tag{4}$$

where,  $P_{Ro}$  is the initial recuperator force,  $V_{Ro}$  is the initial gas volume inside the recuperator,  $A_{PR}$  is the working area of the recuperator piston, and  $n$  is the polytropic exponent whose value is taken as 1.25.

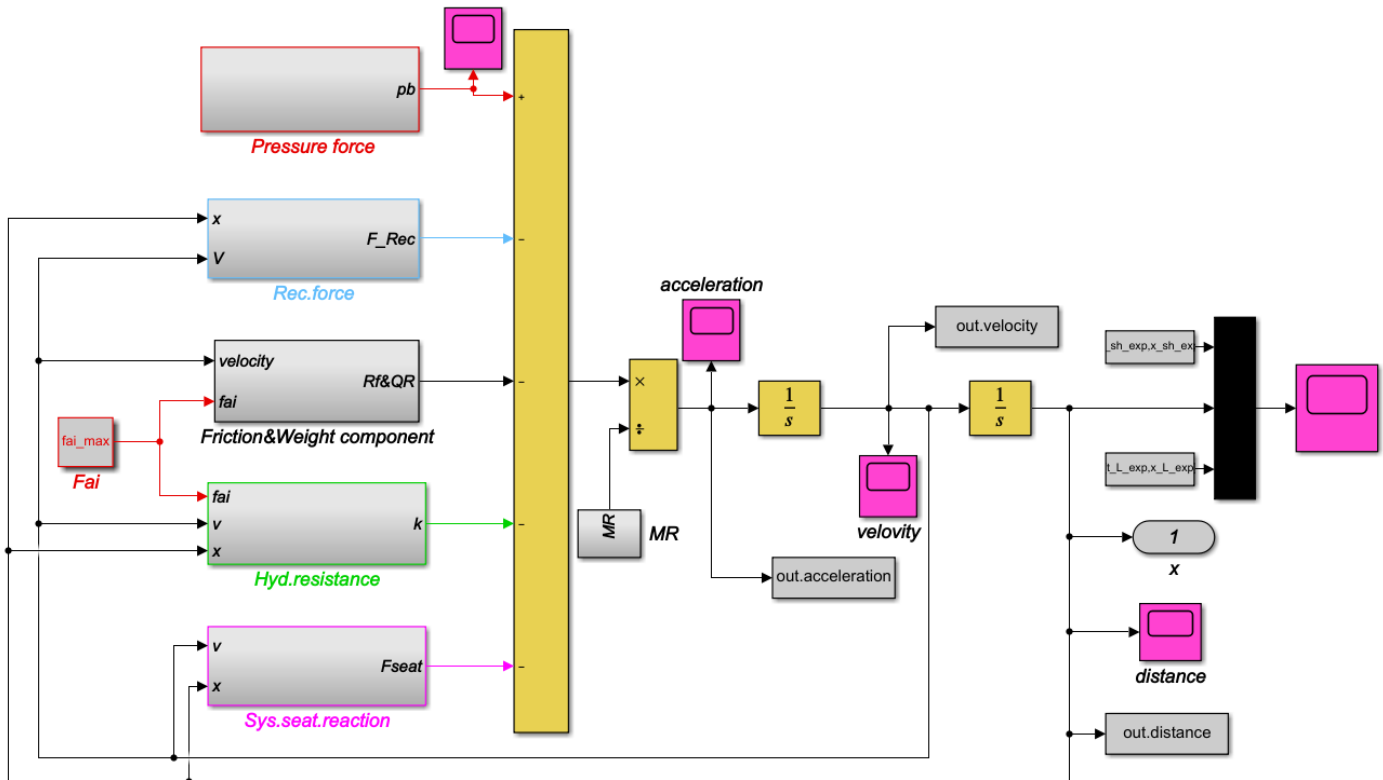


Figure 3. Structure of the mathematical model developed using MATLAB/Simulink.

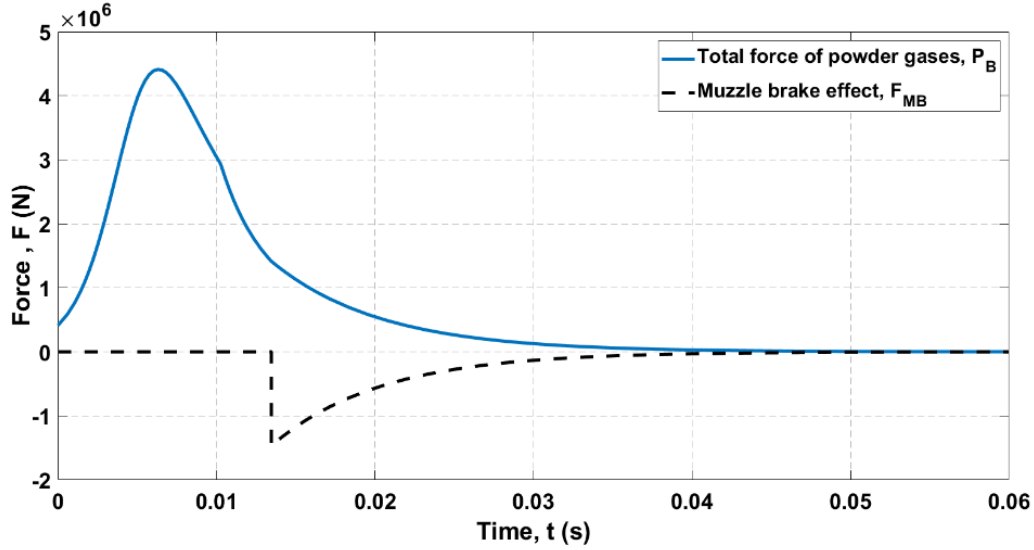


Figure 4. Force of powder gases and effect of muzzle brake.

During recoil,  $F_{rec}$  is expected to be greater than the pressure air force,  $P_{air}$ , due to spring action of the SLV located in the working cylinder, as shown in Fig. 1. On the contrary,  $F_{rec}$  is expected to be smaller than  $P_{air}$  during CR, as the valve closes and the liquid is forced to be throttled from the narrow orifices in the valve causing the pressure in the working cylinder to be smaller than that in the air cylinder.

The recuperator force during recoil can be determined from the equilibrium equation of the forces affecting the valve, as shown in Eqn. (5). The hydraulic losses term during recoil,  $F_{lossesR}$ , is determined using Eqn. (6) presented by Prof. Böswhirth for the study of flow and stability of SLV<sup>17</sup>.

$$F_{rec} = P_{air} + F_{lossesR} + k_{valve} \cdot y \quad (5)$$

$$F_{lossesR} = \xi_1 \cdot \frac{\rho_L \cdot V^2 \cdot A_{PR}}{2} \quad (6)$$

where,  $k_{valve} = 5000$  N is the valve spring stiffness,  $y$  is the valve displacement,  $\xi_1 = 10.5$  is the coefficient of losses during recoil, whose value depends on the ratio between the deflection of the valve and the radius of working cylinder, and  $\rho_L = 1100$  kg/m<sup>3</sup> is the liquid density.

During CR,  $F_{rec}$  is determined, using Eqn. (7). The hydraulic losses term during CR,  $F_{lossesCR}$ , is determined by using the well-known Darcy-Weisbach equation that is commonly used for calculating pressure drop in pipes due to friction<sup>18</sup>, as shown in Eqn. (8).

$$F_{rec} = P_{air} - F_{lossesCR} \quad (7)$$

$$F_{lossesCR} = \frac{f \cdot Lv \cdot \rho_L \cdot v^2}{2 \cdot n_h \cdot d_{vh}} \cdot A_{PR} \quad (8)$$

where,  $f = 0.025$  is a friction factor,  $Lv = 35$  mm is the length of valve hole,  $n_h = 4$  is the number of holes in the SLV,  $v$  is the liquid velocity, and  $d_{vh} = 3$  mm is the hole diameter.

### 3.2 Hydraulic Resistance during Recoil Cycle

The hydraulic resistance during recoil cycle is determined based on applying continuity and Bernoulli's equations to

determine the pressures in the different zones of RM, as shown in Eqn. (9-10)<sup>4-6,19-20</sup>. The following assumptions are adopted: (i) the flow is assumed to be steady, incompressible, and one-dimensional<sup>6,21</sup> (ii) The pressure is homogenous in each zone of the recoil system, (iii) The effects of increase of liquid temperature are neglected, and (iv) the head losses are only proportional to fluid density and flow velocity<sup>6</sup>.

$$\rho_L A v = constant \quad (9)$$

$$p_1 + \frac{\rho_L \cdot v_{F1}^2}{2} = p_2 + \frac{\rho_L \cdot v_{F2}^2}{2} + \xi_2 \cdot \frac{\rho_L \cdot v_{F2}^2}{2} \quad (10)$$

where,  $p_1$  and  $p_2$  are the liquid pressures at two points along the streamline of fluid flow, and  $\xi_2$  is the coefficient of frictional and local losses. Similar equations are applied for the flow between Zone 1 and 3. Thus, the pressures in Zone 1 and Zone 3 can be determined, respectively, as follows<sup>5</sup>:

$$p_1 = C_2 \cdot \left( \frac{A_{PB} - A_{IP}}{A_X} + 1 \right)^2 \cdot V^2 \quad (11)$$

$$p_3 = p_1 - C_3 \cdot \left( \frac{A_{IP}}{\Omega_{min}} \right)^2 \cdot V^2 \quad (12)$$

where,  $\Omega_{min}$  is the minimum area for liquid flow from Zone 1 to 3,  $A_{PB}$  and  $A_{IP}$  are the working areas of RM and CRM pistons, respectively,  $A_X$  is the variable throttling area that depends on both variation of recoil distance and firing angle, and  $C_2$  and  $C_3$  are the recoil constants, whose values depend on the liquid density and frictional and local losses.

During CR, the equation of motion of gun recoiling parts can be written as:

$$m_R \cdot \frac{d^2 X}{dt^2} \approx m_R \cdot \frac{dV}{dt} - P_R - K_C \quad (13)$$

where,  $K_C$  is the total hydraulic resistance affecting CR. This hydraulic resistance evolves from the pressures generated due to fluid flow from Zone 2 to 1 (Flow 21) and from Zone 3 to 1 (Flow 31). These pressures can be expressed, respectively, as follows:

$$p_2 = C_{21} \cdot \left( \frac{A_{2T} + A_x}{A_x} \right)^2 \cdot V^2 \quad (14)$$

$$p_3 = C_{34} \cdot \left( \frac{A_{IP}}{A_{xc}} + 1 \right)^2 \cdot V^2 \quad (15)$$

where,  $A_{2T}$  is the cross-section area of CRM cylinder, and  $A_{xc}$  is the throttling area in CRM.

**4. EXPERIMENTAL MEASUREMENTS**

The experimental measurements of recoil parameters of the 130 mm M-46 FG have been carried out in the Egyptian Central Shooting Ranges (ECSR). The experiments aimed to verify the firing data and measure the time histories of recoil parameters of a new system of the 130 mm M-46 FG that replaces the traditional towed gun with a self-propelled gun. The new self-propelled system adopts the same characteristics of the towed gun system, except for the trails, wheels, and wheel mechanisms. As a result, the measurements of recoil parameters presented in this section also apply to the towed gun systems.

The measuring system is shown in Fig. 5, in which the recoil cycle of the 130 mm FG is recorded using a high-speed camera and a data acquisition system operated with Phantom v9.1 software. The experimental results were carried out at two different angles,  $\phi=20^\circ$  and  $45^\circ$ , to enable measuring the recoil characteristics in case of long and short recoils. The resolution of the high-speed camera was adjusted to 1280x720, and the sampling rate was 1500 frame/s.

The data of the experimental recoil distance was extracted from Phantom v9.1 software by recording the coordinates of a specific point on the recoiling parts during the recoil cycle. The coordinates of two points that represent a standard dimension on the gun (length of recoil cylinder) were used to obtain the scaling factor of recoil displacement. Two frames of the experimental measurements applied for both high and low elevation angles are shown in Fig. 6(a) and (b), respectively.

**5. RESULTS AND DISCUSSIONS**

**5.1 Model Validation**

Figure 7 shows that the theoretical recoil distances are in good agreement with the experimental results at both angles

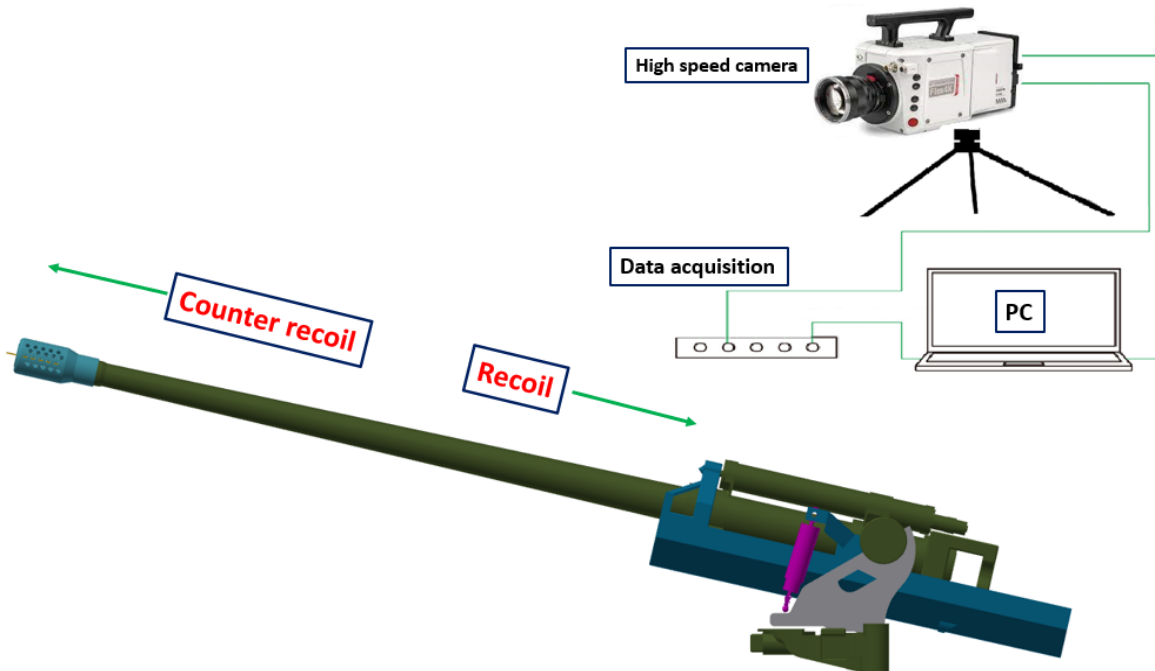


Figure 5. Scheme of the measuring system.



(a)



(b)

Figure 6. Setup of experimental measurements at different elevation angles, (a) Short recoil,  $\phi=45^\circ$ , and (b) Long recoil,  $\phi=20^\circ$ .

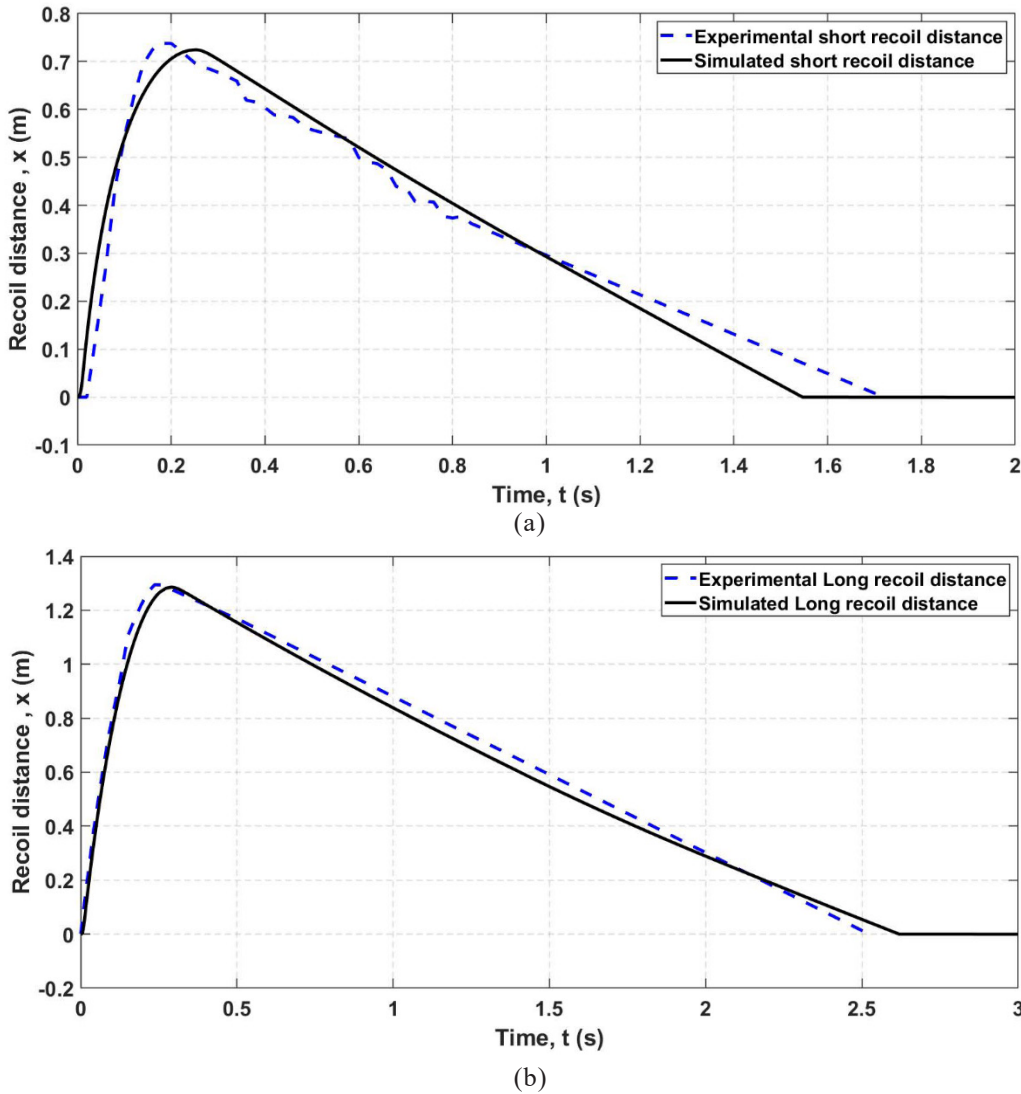


Figure 7. Theoretical and experimental time histories of recoil distance, (a) Short recoil,  $\phi=45^\circ$ , and (b) Long recoil,  $\phi=20^\circ$ .

of elevations. The maximum recoil distance for short recoil is 0.73 m and the total time of the recoil cycle is 1.6 sec. For the long recoil, the maximum recoil distance is 1.26 m, and the total time of the recoil cycle is 2.5 sec. However, it should be noted that due to the limitation of the maximum number of frames captured by the high-speed camera, the experimental measurements do not include the whole recoil period. For the short recoil seen in Fig. 7(a), the experimental measurements were recorded up to 0.85 sec., whereas they were recorded up to 0.7 sec. for the long recoil, as shown in Fig. 7(b). The recoil distance otherwise is assumed to have a linear variation follows the curve fitting of experimental data during CR period. This limitation in the number of frames was compulsory to capture more frames during recoil, as the recoil time is too short in comparison with that of CR. It should be also noted that the values of recoil velocity and resistance are much lower during CR. The maximum relative differences between theoretical and experimental recoil distance are 6.75 % for the short recoil and 7.4 % for the long recoil. These differences are attributed to the assumptions in the mathematical model. In particular, the representation of hydraulic resistance in the mathematical

model as it has the main contribution to the total recoil resistance, and consequently the recoil parameters,  $X$  and  $V$ .

### 5.2 Prediction of Recoil Parameters

Figure 8 displays the recoil velocity predicted for long and short recoils. In both cases, the maximum recoil velocity is approximately 10 m/s. This also agrees with maximum recoil velocities for the case<sup>3,6</sup>. The counter recoil velocity is seen to

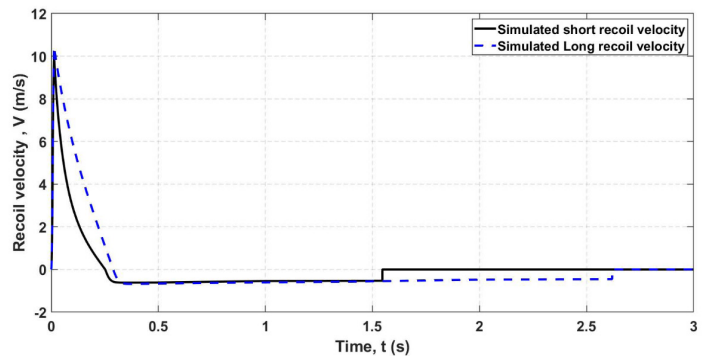


Figure 8. Predicted recoil velocity in case of long and short recoil.

be nearly constant with value of 0.6 m/s. Also, it is noted that the recoiling parts have a nonzero velocity at the end of CR, about 0.4 m/s, which is necessary to ensure complete CR.

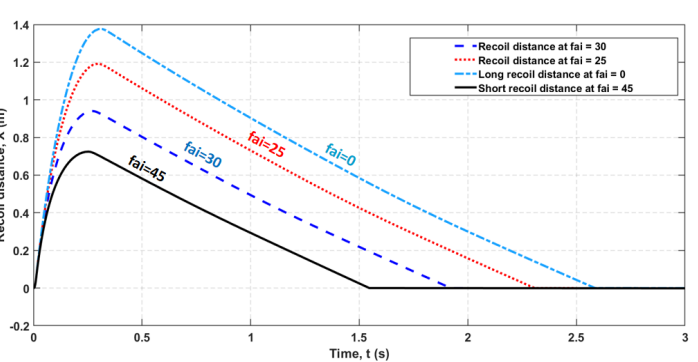
**5.3 Effects of SLV, Elevation Angle and Muzzle Brake Impulse Ratio**

Figures 9, 10 and 11 depict the effect of the presence of SLV in the recuperator during short recoil mode. Figure 9 shows the variation of the actual recuperator force,  $F_{rec}$ , in comparison with the force of air pressure,  $P_{air}$ , according to the mathematical model. It can be noted that the effect of the SLV is very limited during recoil, as the valve is completely opened. However, when the valve closes during CR and the fluid is throttled through the narrow orifices in the SLV, this considerably reduces the force affecting gun recoiling parts. Therefore, the actual driving force of recoiling parts during CR

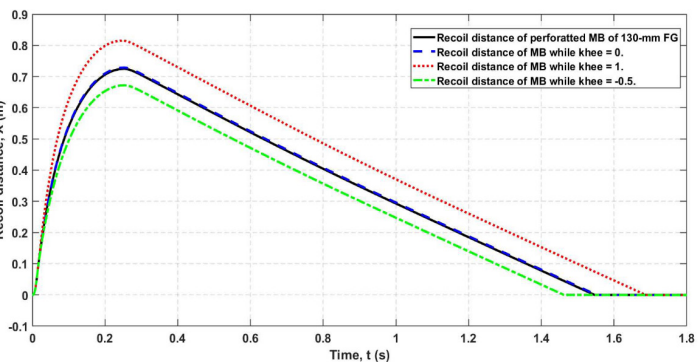
is predicted to be approximately 33 % less than the force of air pressure. This reduction is mainly due to the losses caused due to throttling of liquid through the holes in the SLV.

Figure 10 shows the variation of predicted CR velocity, whereas Fig. 11 presents the corresponding hydraulic resistance with and without consideration of the effect of SLV. Figure 10 shows that the maximum CR velocity is approximately 12 % less than its value without the presence of SLV. As a result, the CR time is found to be about 10 % greater and the impact velocity at end of CR is 11 % less. The predicted CR velocity due to existence of the effect of SLV is also supported by the experimental data shown in Fig. 7(a), where the CR velocity is represented by the gradient of CR displacement has an average value of 0.6 m/s. It should be noted that preserving a reasonable value of impact velocity at end of CR is compulsory to secure complete CR, as it may cause serious errors during firing of next rounds. On the other hand, the corresponding maximum hydraulic resistance during CR seen in Fig. 11 is predicted to be reduced by about 20 % due to the effect of SLV. Also, it is worth mentioning that the recoil velocity and displacement have almost the same values either with or without considering the effect of SLV, which is due to the very limited of SLV during recoil.

The variations of recoil displacement at four different elevation angles are shown in Fig. 12. The four angles represent all recoil modes, namely short recoil ( $\phi=45^\circ$ ), intermediate recoil ( $\phi=25^\circ$  and  $30^\circ$ ), and long recoil ( $\phi=0^\circ$ ). It can be concluded that the maximum recoil distance and the total time of recoil increase when firing at lower elevation angles. These variations are due to the different values of throttling area operated in each mode of recoil, and this also leads to variation of total recoil resistance.



**Figure 12. Variation of recoil distance with respect to elevation angle.**



**Figure 13. Effect of variation of impulse ratio ( $\chi$ ) on recoil distance.**

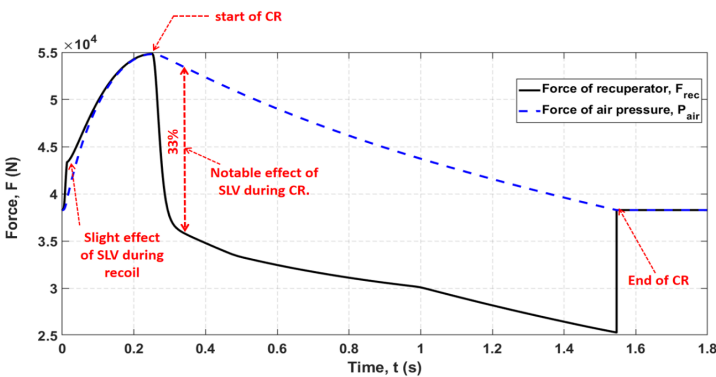


**Figure 9. Recuperator and air pressure forces.**

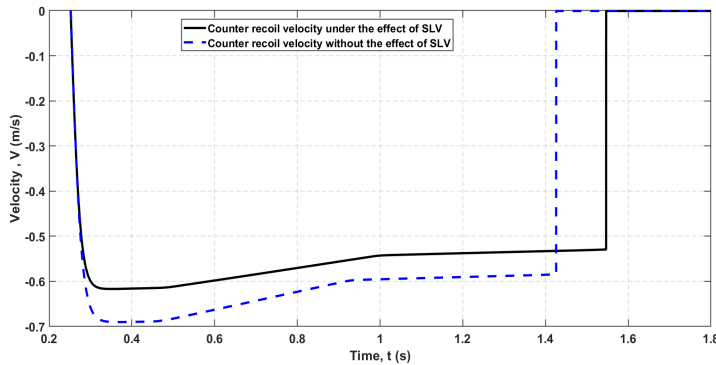


**Figure 10. Effect of SLV on counter recoil velocity.**

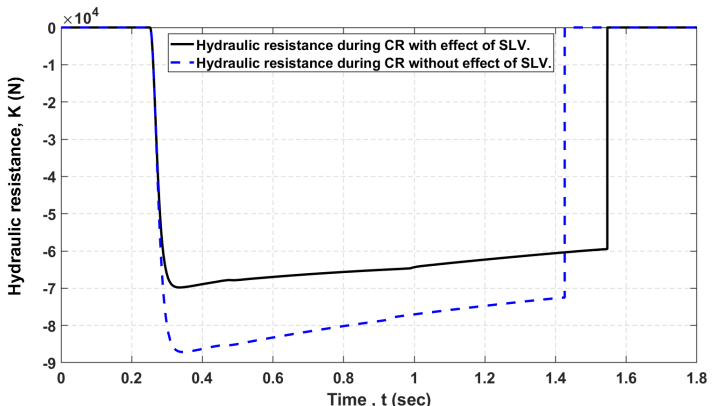


**Figure 11. Effect of SLV on hydraulic resistance during counter recoil.**

The muzzle brake has a great effect on gun recoil parameters<sup>15</sup>. Its effect is taken into consideration by determination of the impulse ratio,  $\chi$ . Figure 13 shows the effect of using different values of impulse ratio on the recoil distance. It is seen that, when  $\chi=1$  (there is no muzzle brake), the recoil distance is of maximum value. The smaller values of  $\chi$  conduce more effective muzzle brakes and shorter recoil distances are obtained.

## 6. CONCLUSION

The dynamic characteristics of gun recoil system provided with Spring-Loaded Valve (SLV) and variable recoil mechanism are analysed based on theoretical and experimental approaches. The results of calculated recoil parameters using the presented mathematical model are in a very good agreement with the measured values. It can be concluded that the presence of SLV in hydro-pneumatic recuperators has a considerable effect on the variation of recoil parameters. This effect mainly exists during CR rather than recoil. The driving force of gun recoiling parts during CR reduces by about 33 % compared to the pressure force of compressed air in the recuperator. Consequently, the CR velocity also reduces by approximately 11 %, the CR time period increases by 10 %, and the hydraulic resistance against CR reduces by about 20 %. The current mathematical approach gives an insight into necessity of including the effect of SLV in modelling of similar gun hydraulic gun systems such as recoil brakes, recuperators, and potentially in equilibrators.

## REFERENCES

- Ahmadian, M.; Appleton, R. & Norris, J. An analytical study of fire out of battery using magneto rheological dampers. *Shock & Vib.*, 2002, **9**, 129-142. doi:10.1155/2002/983140.
- US Department of Defense. Recoil Systems. Military Handbook No. DOD-HDBK-778. Washington, 1988.
- Elsaady, W.; Ibrahim, A. & Abdalla, A. Numerical simulation of flow field in coaxial tank gun recoil damper. *Adv. Mil. Technol.*, 2019, **14**, 01287. doi:10.3849/aimt.01287.
- Xiaodong, Z.; Peilin, Z.; Jianping, F. & Cheng, W. Research on according calculation of hydraulic resistance coefficients for recoil brake of gun based on improved genetic algorithm. *In Proceedings of International Conference on MTMA, Hunan, China, 2009.* doi: 10.1109/ICMTMA.2009.552.
- Elsaady, W.; Ibrahim, A.; Abdalla, A. & Hussien, A. Dynamic simulation of tank gun recoil cycle. *In Proceedings of International Conference on AMME, Cairo, 2014.* doi: 10.21608/AMME.2014.35481.
- Balla, J.; Krist, Z. & Melsa, P. Study of movement of 125 mm tank cannon recoiling parts. *In Proceedings of International Conference of MT, Brno, Czech Republic, 2021.* doi: 10.1109/ICMT52455.2021.9502783.
- Miao, W.; Qian, L. & Chen, L. Hydraulic node model and parameter identification of a dull recoil brake. *J. Mech. Sci. Technol.*, 2022, **36**, 5511-5521. doi: 10.1007/s12206-022-1016-7.
- Shu-qi, G. & Bao-lin, H. Simulation and parameters intelligent optimization of soft recoil system. *In Proceedings of Chinese Automation Congress, Shanghai, China, 2020.* doi: 10.1109/CAC51589.2020.9326926.
- Zhang, G.; Wang, H.; Qing, O. & Wang, J. Numerical analysis of multi-physical field for independent three-stage magnetorheological damper of double rod during recoil process of artillery. *Mech. Eng. Sci.*, 2019, **233**, 4960-4979. doi:10.1177/0954406219838583.
- Ouyang, Q.; Zheng, J.; Li, Z.; Hu, M. & Wang, J. Controllability analysis and testing of a novel magnetorheological absorber for field gun recoil mitigation. *Smart Mat. & Struc.*, 2016, **25**, 115041. doi:10.1088/0964-1726/25/11/115041.
- Singh, H.; Hu, W.; Wereley, N. & Glass, W. Experimental validation of a magnetorheological energy absorber design optimized for shock and impact loads. *Smart Mat. & Struc.*, 2014, **23**, 352-363. doi: 10.1088/0964-1726/23/12/125033.
- Huan, T.; Jianzhong, W. & Jinzhong, Z. Simulation and analysis of flow field in recoil mechanism based on elastic colloid. *In Proceedings of WASE International Conference on IE, BeiDai, China, 2010.* doi:10.1109/ICIE.2010.238.
- Kang, K.; & Gimm, H. Numerical and experimental studies on the dynamic behaviours of a gun that uses the soft recoil system. *J. Mech. Sci. Technol.*, 2012, **26**, 2167-2170. doi: 10.1007/s12206-012-0538-9.
- Rao, K. & Sharma, K. Art in internal ballistics, 1982, *Def. Sci. J.*, **32**, 157-174.
- Sherif, M.; Abdelsalam, O.R. & Aboul, M. Design optimisation of muzzle brake for sniper rifle. *Def. Sci. J.*, 2018, **68**(5) 438:444. doi: 10.14429/dsj.68.12754.
- Svete, A.; Bajsić, I. & Kutin, J. Investigation of polytropic corrections for the piston-in-cylinder primary standard used in dynamic calibrations of pressure sensors. *Sensors & Actuators A: Physical*, 2018, **274**, 262–271. doi: 10.1016/j.sna.2018.03.019.
- Boswirth, L. Flow forces and the tilting of spring-loaded valve plates - Part I. *In Proceedings of International Compressor Engineering Conference, USA, 1980.* https://docs.lib.purdue.edu/icec.
- Kundu, P. & Cohen, I. Fluid Mechanics. Elsevier, USA 2016.
- Lin, T.; Ping, H.; Yang, T.; Chan, C. & Yang, C. Dynamic Simulation of the Recoil Mechanism on Artillery Weapons. *In Proceedings of International Conference of Computer Engineering Systems, Cairo, Egypt, 2009.* doi: 10.1109/ICCES15835.2009.
- Xiaodong, Z.; Peilin, Z.; Jianping, F. & Cheng, W. A Method of recoil brake interior chamber pressure test and calculation on gun's recoiling impact. *In Proceedings of*

International Conference on EMI, Beijing, China, 2009.  
doi: 10.1109/ICEMI.2009.5274450.

21. Changlin, Ma; Feng, Li. & Hao, Lin. Mechanism modelling and Simulink simulation analysis of digital hydraulic cylinder. *In* Proceedings of 2<sup>nd</sup> International Conference on CMSA, Zhuhai, China, 2020.  
doi:10.1088/1742-6596/1624/2/022010.

## CONTRIBUTORS

**Mr Mohamed Abdullah** is graduated from Department of Weapons and Ammunition, Military Technical College, Cairo, Egypt. His research interests are: Modelling and analysis of gun recoil systems using analytical and numerical techniques. In the current study, he is involved in model setup, major contribution in paper writing, literature review, and elaboration of drawings.

**Dr Wael Elsaady** obtained his PhD degree in Mechanical Engineering from The University of Manchester, UK. His research interests involve: Gun recoil systems, design of gun systems, magneto-rheological dampers, CFD techniques involving

single and two phase flow, finite element modelling.

In the current study, he is involved in revising and enhancing the mathematical model, experimental measurements, and revision and organisation of the paper.

**Dr Ahmed Ibrahim** obtained his PhD degree in Mechanical Engineering from the University of Manchester, UK in 2007. Now, he is working as an Associate Professor in the Department of Weapons and Ammunition at Military Technical College. His researches are specialised in the field of studying the aerodynamics of projectiles and CFD methods applied to this field of study.

In the current research, he has supervised the research work to get this article in its final form.

**Dr Ibrahim Elsharif** is a Professor in the Military Technical College, Cairo Egypt. He obtained his PhD in adaptive control of hydraulic systems from Alabama University, USA in 1995. His research interest include: Power hydraulics, mechatronics, robotics, and automatic control.

In the current research, he has supervised experimental work, and provided revision of the paper.